

Article

The Rhodamine–Perylene Compact Electron Donor–Acceptor Dyad: Spin-Orbit Charge-Transfer Intersystem Crossing and the Energy Balance of the Triplet Excited States

Muhammad Imran [†] , Dongyi Liu [†] , Kaiyue Ye , Xue Zhang and Jianzhang Zhao ^{*} 

State Key Laboratory of Fine Chemicals, Frontiers Science Center for Smart Materials Oriented Chemical Engineering, School of Chemical Engineering, Dalian University of Technology, E-208 West Campus, 2 Ling Gong Rd., Dalian 116024, China

* Correspondence: zhaojzh@dlut.edu.cn

[†] These authors contributed equally to this work.

Abstract: We prepared a rhodamine (RB)–perylene (Pery) compact electron donor/acceptor dyad (**RB–Pery**) to study the spin-orbit charge-transfer intersystem crossing (SOCT–ISC). The UV–vis absorption spectrum indicates a negligible electronic interaction between the donor and acceptor at ground state. However, the fluorescence of both the RB and Pery units are quenched in the dyad, which is attributed to the photoinduced electron transfer, supported by the electrochemical studies. Nanosecond transient absorption (ns-TA) spectra show delocalized triplet states, i.e., there is an excited-state equilibrium between Pery and the RB triplet states. The triplet state lifetime was determined as 109.8 μ s. With intermolecular triplet–triplet energy transfer, monitored using ns-TA spectra, the triplet-state energy balance between RB and Pery in **RB–Pery** was confirmed. The proposed cascade photophysical processes of the dyad are $^1\text{RB}^*\text{-Pery} \rightarrow \text{RB-Pery}^+\bullet \rightarrow [^3\text{RB}^*\text{-Pery} \leftrightarrow \text{RB-}^3\text{Pery}^*]$. Moreover, long-lived rhodamine radical cation (in milliseconds) was detected in both deaerated/aerated non-polar or low-polarity solvents (i.e., *p*-xylene, toluene). The potential energy curve of the dyad against the variation in the dihedral angle between the two units indicates large torsional freedom ($53^\circ \sim 128^\circ$) in **RB–Pery**, which leads to inefficient SOCT–ISC; consequently, low singlet-oxygen quantum yields ($\Phi_\Delta = 2 \sim 8\%$) were observed.



Citation: Imran, M.; Liu, D.; Ye, K.; Zhang, X.; Zhao, J. The Rhodamine–Perylene Compact Electron Donor–Acceptor Dyad: Spin-Orbit Charge-Transfer Intersystem Crossing and the Energy Balance of the Triplet Excited States. *Photochem* **2024**, *4*, 40–56. <https://doi.org/10.3390/photochem4010004>

Received: 30 December 2023

Revised: 23 January 2024

Accepted: 24 January 2024

Published: 29 January 2024



Copyright: © 2024 by the authors. Licensee MDPI, Basel, Switzerland. This article is an open access article distributed under the terms and conditions of the Creative Commons Attribution (CC BY) license (<https://creativecommons.org/licenses/by/4.0/>).

Keywords: electron transfer; intersystem crossing; nanosecond transient absorption spectroscopy; perylene; triplet-state equilibrium

1. Introduction

The formation of long-lived triplet states in triplet photosensitizers (PSs) is of great importance due to their potential applications in photocatalysis [1–4], optical limiting [5], molecular probes [6], and triplet–triplet annihilation upconversion [3,4,7,8]. Conventional triplet PSs contain heavy atoms to enhance the intersystem crossing (ISC), for instance, Pt, Ir, Ru or I, Br, etc. [3,9–11]. However, these triplet PSs suffer from the drawbacks of high cost and toxicity and a shortened triplet-state lifetime due to the strong spin-orbit coupling effect. In order to address these challenges, in recent years, numerous heavy-atom-free triplet PSs have been developed. Some methods used in designing heavy-atom-free triplet PSs to show predetermined efficient ISC include using an electron spin converter [12–14], singlet fission [15,16], exciton coupling [17], or radical enhanced ISC [8,18]. The charge recombination (CR)-induced ISC via radical pair ISC (RP-ISC) mechanism in electron donor/acceptor dyads is also known, but the electron donor and acceptor are separated by a large distance and the ISC efficiency is usually low [19,20]. However, most of these triplet PSs are synthetically demanding; for instance, a special orientation of the chromophores for the exciton coupling-induced ISC is required [21], whereas the dyads showing RP-ISC require long and rigid

linkers, which make the synthesis challenging. Therefore, a simple molecular structural motif for the design of triplet PSs showing efficient ISC is highly desired.

Recently, it was found that efficient ISC may occur in compact electron donor/acceptor dyads if the electron donor and acceptor adopt orthogonal geometry. Under this circumstance, the CR is accompanied by molecular orbital angular momentum change, which offsets the electron spin angular momentum change of the ISC. Consequently, the ISC is enhanced by the CR in these orthogonal compact electron donor/acceptor dyads [22,23]. This so-called spin-orbit charge transfer ISC (SOCT-ISC) mechanism actually complies with the spirit of El Sayed's rule for ISC. These compact electron donor/acceptor dyads showing SOCT-ISC have advantages of simple molecular structures, feasible preparation, and high ISC yields. The molecular structures and the photophysical properties can be feasibly tuned by using different electron donors/acceptors. Previously, a bodipy–anthracene dyad was reported to show efficient triplet formation (triplet quantum yield~90%) and a long-lived triplet state (85 μ s) via SOCT-ISC [24]. This SOCT-ISC was also studied with other electron donor–acceptor systems, for instance, anthryl/phenothiazine [25], Bodipy/phenothiazine [26], perylene (Pery)/Bodipy [27], Pery/phenothiazine [28], perylenemonoimide/phenothiazine [29], perylenemonoimide/carbazole [30], and naphthaimide/Pery [31]. However, rhodamine B (RB) is rarely used in electron donor/acceptor dyads showing SOCT-ISC [32–34].

The RB moiety is a well-known and versatile fluorophore that shows strong absorption and emission in the visible spectral region; its derivatives have been used extensively for fluorescent molecular probes and fluorescent bioimaging [35–39]. Recently, rhodamine moiety has been used as a light-harvesting unit in transition-metal complexes [40–42], as well as for the application of the triplet state in TTA upconversion [43], photodynamic therapeutic studies [44], or one-photon excitation molecular upconversion [45–47]. However, rhodamine was not used for the preparation of electron donor/acceptor dyads showing SOCT-ISC. Since rhodamine shows strong absorption of visible light and is used as a strong electron acceptor (oxidation potential (E_{OX}) = +0.87 V vs. Fc/Fc⁺), it will be interesting to study the amplification of rhodamine in electron donor/acceptor dyads showing SOCT-ISC.

Herein, we use Pery as an electron donor and cationic RB, a well-known xanthene-based dye, as an electron acceptor, to synthesize an **RB–Pery** compact dyad with favourable geometry to achieve SOCT-ISC. Note that the rhodamine part is positively charged, the electron transfer is actually a charge shift, and there is no Coulombic interaction in the resulting state. Steady-state absorption/emission spectroscopies, time-resolved transient absorption spectroscopy, and electrochemical and density functional theory (DFT) computations have been used to study the photophysical properties of the compounds. Triplet-state equilibrium was observed with nanosecond transient spectra showing a delocalized triplet state. Also, a long-lived rhodamine radical cation (~10 ms) was detected in non-polar solvents.

2. Materials and Methods

2.1. General Methods

UV–vis absorption spectra were measured on an Agilent 8453 UV–vis spectrophotometer (Agilent Ltd., Santa Clara, CA, USA). Fluorescence emission spectra were recorded on an RF-5301PC spectrofluorometer (Shimadzu Ltd., Kyoto, Japan). Luminescence lifetimes were measured on an OB920 fluorescence/phosphorescence lifetime spectrometer (Edinburgh Instruments Ltd., Livingston, UK). The fluorescence quantum yields were measured with an absolute photoluminescence quantum yield spectrometer (Quantaaurus-QY Plus C13534-11, Hamamatsu Ltd., Hamamatsu, Japan).

2.2. Synthesis of Compound RB–Pery

A mixture of 3-perylenecarboxaldehyde (140 mg, 0.5 mmol), 3-(diethylamino)phenol (200 mg, 1.2 mmol), *p*-TsOH (18 mg, 0.1 mmol), and AcOH (7 mL) was heated at 90 °C and stirred for 12 h. Then, the reaction mixture was cooled to room temperature and the pH of the mixture was adjusted to above 7 with a 10% NaOH solution. The precipitate was

filtered and washed with water (20 mL). Then, the solid was dissolved in CH₂Cl₂ (10 mL) and chloranil (62 mg, 0.25 mmol) was added. The mixture was stirred for 4.5 h. After the removal of the solvent, the residue was purified via column chromatography (silica gel; CH₂Cl₂/methanol, 20:1, *v/v*) to give a purple solid, 15 mg (yield: 5.0%). ¹H NMR (400 MHz, CDCl₃, ppm) δ 8.37–8.38 (d, *J* = 4.0 Hz, 1H), 8.32–8.34 (d, *J* = 8.0 Hz, 1H), 8.26–8.27 (d, *J* = 4.0 Hz, 2H), 7.78–7.82 (dd, 2H), 7.54–7.60 (q, 2H), 7.40–7.45 (m, 2H), 7.22–7.25 (d, *J* = 8.0 Hz, 2H), 7.15–7.17 (d, *J* = 8.0 Hz, 1H), 6.95 (s, 2H), 6.79–6.82 (d, *J* = 12.0 Hz, 2H), 3.65–3.66 (q, 8H), 1.33 (t, *J* = 12.0 Hz, 12H); ¹³C NMR (CDCl₃, 100 MHz): δ 158.0, 156.7, 155.7, 134.6, 133.8, 133.0, 132.0, 131.9, 130.4, 130.1, 129.2, 128.8, 128.7, 128.6, 128.5, 128.1, 126.9, 126.9, 124.9, 121.4, 121.3, 121.0, 119.4, 114.2, 114.1, 96.6, 77.4, 77.3, 77.1, 76.8, 46.3, 29.7, 12.7. ESI–HRMS (C₄₁H₃₇N₂O⁺): Calcd, *m/z* = 573.2900; found, *m/z* = 573.2909.

2.3. Singlet Oxygen Quantum Yield Measurements

The determination of the singlet oxygen quantum yields (Φ_{Δ}) of the compounds was carried out using the chemical trapping method; 1,3-diphenylisobenzofuran (DPBF) was used as the singlet oxygen (¹O₂) scavenger. The air-saturated mixture solution of the compounds and DPBF were irradiated at an appropriate wavelength (with a Xe lamp/monochromator) and the ¹O₂ production was monitored by following the absorbance of DPBF at ca. 414 nm, which was recorded with the UV–2550 spectrophotometer. Rose Bengal (Φ_{Δ} = 76% in MeOH) and Ru(bpy)₃(PF₃)₂ (Φ_{Δ} = 57% in dichloromethane, DCM) were used as standards. The absorbance at the excitation wavelength was the same for the reference and compounds; for this purpose, optically matched solutions were used. The Φ_{Δ} values were calculated using Equation (1).

$$\Phi_{\Delta, \text{sample}} = \Phi_{\Delta, \text{standard}} \left(\frac{1 - 10^{-A_{\text{standard}}}}{1 - 10^{-A_{\text{sample}}}} \right) \left(\frac{m_{\text{sample}}}{m_{\text{standard}}} \right) \left(\frac{\eta_{\text{sample}}}{\eta_{\text{standard}}} \right)^2 \quad (1)$$

where *A* is the absorbance at the excitation wavelength, *m* is the slope of the plot of absorbance of DPBF at 414 nm versus the irradiation time, and η is the refractive index of the solvent used for the measurements.

2.4. Nanosecond Time-Resolved Transient Absorption Spectroscopy

An LP980 laser flash photolysis spectrometer (Edinburgh Instruments Ltd., Livingston, UK) was used to record the ns-TA spectra of the compounds. An optical parametric oscillator (OPO, tuneable between 210 and 710 nm) was used as the pulse laser excitation source, and the probe source was a 150 W ozone-free xenon arc lamp (pulsed mode up to 10 Hz). The typical laser pulse energy was ca. 5 mJ per pulse. The transmission properties of the sample before, during, and after the exciting pulse were converted by the detector into electrical signals that were measured with an oscilloscope (TDS 3012C, 100 MHz). For all measurements, the sample was placed in a quartz cuvette (10 mm optical path). Before measurements, all sample solutions were purged with N₂ for ca. 15 min. The recorded kinetic traces and transient spectra were analysed using the L900 software. (<https://www.edinst.com/products/l900-software/>, access on 15 December 2023). The triplet–triplet energy transfer (TTET) method was used to verify the triplet excited-state equilibrium with the photosensitizer mixed with the compounds, and the transient spectra were analysed with global fitting using the Glotarn software, version 1.5.1 (sequential model).

2.5. Electrochemical Measurements

Cyclic voltammetry (CV) curves were obtained on a CHI610D electrochemical workstation (CHI Instruments, Inc., Shanghai, China). The electrochemical setup consists of two main parts, i.e., (i) an electrochemical workstation and (ii) an electrolytic cell compartment. The electrolytic cell compartment has three electrodes: one working electrode, a reference electrode, and a counter electrode. Under deaerated conditions, a glassy carbon electrode was used as the working electrode. A silver nitrate-containing (Ag/AgNO₃) silver electrode as the reference electrode and a platinum electrode was used as a counter electrode. DCM

was used as the solvent and ferrocene was the internal reference for all the CV measurements. The tetrabutyl hexafluoroammonium phosphate ($\text{Bu}_4\text{N}[\text{PF}_6]$, 0.10 M) was used as a supporting electrolyte. After connecting the electrolytic cell to the electrochemical workstation, a scan was performed at a scan rate of 50 mV s^{-1} . Then, by recording the current value under different voltages, the cyclic voltammetry curves were obtained. For reversible peaks, the potential values were taken as the average value of the anode peak potential and the cathode peak potential, and the ferrocene peak was adjusted at 0 V in the cyclic voltammograms.

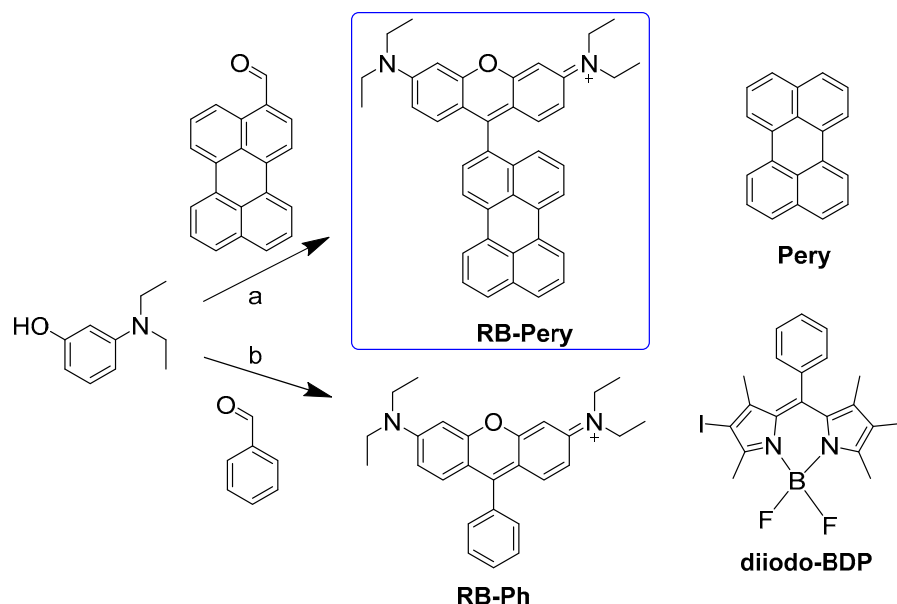
2.6. DFT Calculations

The geometries of the compounds were optimized by using DFT with the B3LYP functional and 6-31G (d) basis set. The excitation energy and energy gaps between the S_0 state and the excited triplet states of the compounds were computed using time-dependent density functional theory (TD-DFT), which is based on the optimal ground-state geometry. All the calculations were performed with the Gaussian 09W program [48].

3. Results and Discussion

3.1. Molecular Structure Design and Synthesis

Previously, a neutral spiro lactam rhodamine moiety was used as an electron donor in the construction of SOCT-ISC dyads [49,50]. However, the positively charged xantheno moiety is rarely used in SOCT-ISC dyads. On the other side, arenes can be used as electron donors to achieve decent SOCT-ISC efficiency [31,51]. Herein, we directly connected the cationic rhodamine moiety with perylene unit via a C-C bond and obtained an **RB-Pery** dyad (Scheme 1). In this molecular system, the positively charged rhodamine unit acts as an electron acceptor/visible-light-harvesting chromophore, and the perylene unit is the electron donor. Unsubstituted perylene and rhodamine substituted with a phenyl group (**RB-Ph**) are the two reference compounds for this study.



Scheme 1. Synthesis of RB derivatives: (a) p -TsOH, AcOH, 90°C , 12 h; DCM, chloranil, reflux, 4.5 h, yield: 5%. (b) p -TsOH, AcOH, 70°C , 7 h; DCM, chloranil, rt, 2 h, yield: 15%. The molecular structures of two reference compounds of Pery and 2,6-diiodo-BDP used in the study are also presented.

The synthesis of the target compounds was based on the reported methods [43]; all the chemicals used in the synthesis were analytically pure. The molecular structures of the compounds were verified with ^1H , ^{13}NMR , and HRMS characterization (see experimental section and supporting information).

3.2. Density Functional Theory (DFT) Calculations

The ground-state geometry of the dyad was optimized with DFT (Figure 1a). The dihedral angle between perylene and rhodamine moieties is 69.0° , which is supposed to be beneficial for the occurrence of SOCT-ISC [25,52–54]. However, low singlet-oxygen quantum yields of **RB-Pery** were obtained only in two solvents, i.e., 2.7% in toluene (TOL), 8% in *p*-xylene (*p*-XYL), and none in other solvents (see Table S3). In this case, the related potential energy curve (PEC) of **RB-Pery** against the torsion angle between the perylene and the rhodamine units was constructed with DFT optimization (Figure 1b), showing that the energy remains minimum under the room temperature thermal energy range (<0.026 eV) when the rotational dihedral angles ($\angle C4-C7-C51-C53$) vary from 53° to 128° , indicating large rotation freedom in **RB-Pery**, and this may lead to inefficient SOCT-ISC.

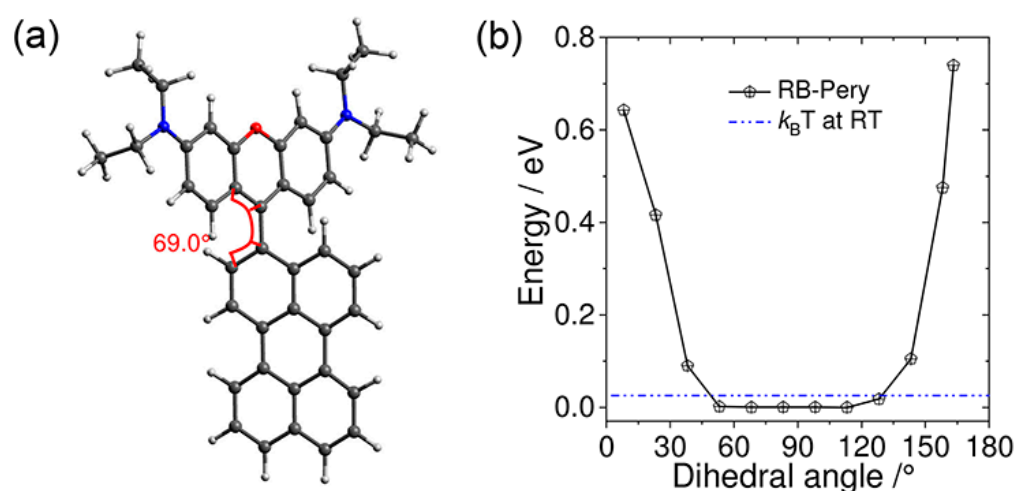


Figure 1. (a) The ground-state optimized geometry with a dihedral angle indicated (between C4–C7–C51–C53 atoms) of **RB-Pery** and (b) the ground-state potential energy curve (as a function of the rotational dihedral angle about the C–C connection between donor and acceptor units in **RB-Pery**). The blue dotted line denotes the thermal energy of room temperature (0.026 eV). Calculated using DFT (B3LYP/6-31G(d)) level with Gaussian 09.

The frontier molecular orbitals of compounds at the ground state were studied (Figure 2). The highest occupied molecular orbital (HOMO) of **RB-Pery** is completely confined on the perylene unit; in contrast, the lowest unoccupied molecular orbital (LUMO) is localized on the xantheno moiety. Therefore, the transition from HOMO→LUMO of **RB-Pery** is a CT feature that shows the possibility of intramolecular electron transfer (charge or hole shift) in the dyad upon photoexcitation. The result also indicates that perylene is an electron donor and xantheno is an electron acceptor in the dyad. On the other side, the HOMO and LUMO of the reference, **RB-Ph**, are mostly localized on the xantheno unit; thus, electron transfer is unlikely, although the phenyl moiety acts as electron donor in naphthalenediimide derivatives [55]. The triplet excited-state spin density of **RB-Pery** is delocalized on the entire molecule (Figure 2), indicating the possibility of energy balance or interconversion between the rhodamine triplet state ($^3\text{RB}^*$) and perylene triplet state ($^3\text{Pery}^*$) in **RB-Pery**.

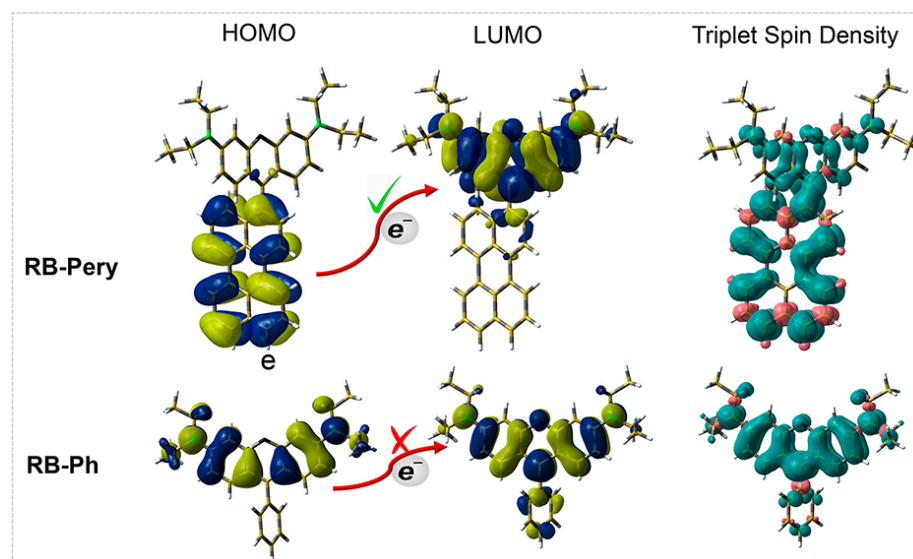


Figure 2. The ground-state electron spin-density distributions of the HOMO/LUMO and triplet-state spin-density distributions of **RB-Pery** and **RB-Ph**. Isovalues are 0.001. All the calculations were based on the DFT (B3LYP/6-31G(d)) level with Gaussian 09.

3.3. UV-Vis Absorption and Fluorescence Emission Spectra

The steady-state UV-vis absorption and emission spectra of the compounds were studied (Figure 3a). A typical structured absorption profile was observed for Pery in the range of 350–450 nm. Similar absorption bands were observed in **RB-Pery** but with smaller magnitudes. The absorption of the rhodamine moiety at 575 nm is similar to the reference, **RB-Ph**, indicating the negligible interaction between two moieties at the ground state. The fluorescence emission spectra of **RB-Pery** and Pery were compared (Figure 3b; optically matched solutions were used). The fluorescence of Pery is at 443 nm with significant vibration progress. For **RB-Pery**, however, the emission of the Pery unit is strongly quenched (note that the perylene part is selectively excited). This quenching may be due to singlet energy transfer or charge transfer to the acceptor unit. Similarly, the fluorescence of **RB-Pery** and **RB-Ph** is compared (Figure 3c). In this case, the fluorescence of the rhodamine unit in **RB-Pery** at 598 nm is weaker than that of **RB-Ph**. The fluorescence quantum yields of the two compounds are 2.4% and 14.2%, respectively (Table 1). This reduced fluorescence quantum yield for the rhodamine unit in the dyad is attributed to the intramolecular charge transfer process.

Table 1. Photophysical parameters of the compounds ^a.

Compounds	λ_{abs}^b (nm)	ϵ^c	λ_{em}^d (nm)	Φ_{Δ}^e (%)	Φ_{F}^f (%)	τ_{F}^g (ns)	τ_{T}^h (μs)
Pery	438	4.2	443	4.8 ± 0.5	77.7	3.9 ± 0.5	596 ± 5^i
RB-Ph	567	7.0	590	– ^j	14.2	1.3 ± 0.5 (97%) 8.5 ± 0.5 (3%)	– ^j
RB-Pery	445, 575	2.2, 6.3	453, 598	8.0 ± 1	2.4 (RB), 6.0 (Pery)	3.3 (96%) 16.7 (4%) \pm 0.2	109.8 ± 5

^a In TOL, $c = 1.0 \times 10^{-5}$ M, 25 °C. ^b Absorption maxima. ^c Molar absorption coefficient at absorption maxima, $\epsilon: 10^4 \text{ M}^{-1} \text{ cm}^{-1}$. ^d Maximal emission wavelength, $\lambda_{\text{ex}} = 415$ nm, $A = 0.10$, 25 °C. ^e Singlet oxygen quantum yield in *p*-XYL; Rose Bengal was used as standard ($\Phi_{\Delta} = 76\%$ in MeOH) for **RB-Ph** and **RB-Pery**; $\text{Ru}(\text{bpy})_3(\text{PF}_6)_2$ was used as standard ($\Phi_{\Delta} = 57\%$ in DCM) for Pery. ^f Absolute photo-luminescence quantum yield; error bar: $\pm 0.1\%$; Pery and **RB-Pery** ($\lambda_{\text{ex}} = 415$ nm), **RB-Pery** ($\lambda_{\text{ex}} = 506$ nm), $A = 0.10$. ^g Luminescence lifetime, $\lambda_{\text{ex}} = 405$ nm. ^h Triplet excited-state lifetime determined with nanosecond transient absorption spectroscopy in DCM. ⁱ Lifetime of the perylene radical cation determined with nanosecond transient absorption spectroscopy in deaerated DCM. ^j Not observed.

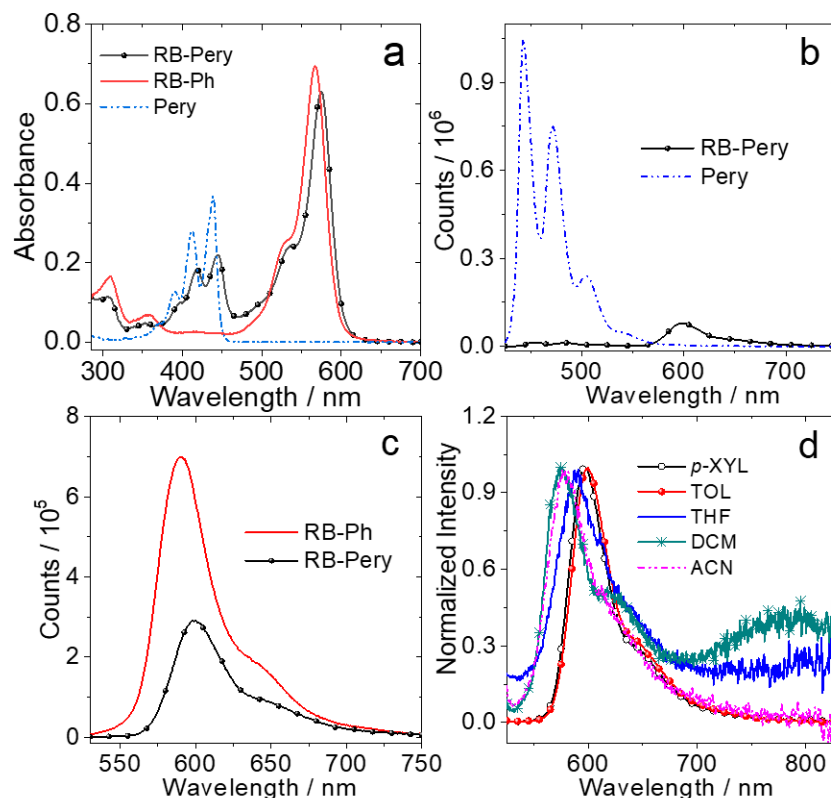


Figure 3. (a) UV-vis absorption spectra of the compounds in TOL; $c = 1.0 \times 10^{-5}$ M. (b) Comparison of the fluorescence emission spectra of Pery and **RB-Pery** with $\lambda_{\text{ex}} = 415$ nm. (c) Comparison of the fluorescence emission spectra of **RB-Ph** and **RB-Pery** with $\lambda_{\text{ex}} = 520$ nm; note that in both cases, optically matched solutions were used ($A = 0.10$; in TOL). (d) Normalized emission spectrum of **RB-Pery** in different solvents. $\lambda_{\text{ex}} = 520$ nm. 25 °C.

The emission intensity of **RB-Pery** decreased as the solvent polarity increased (Figure S7a). The normalized emission spectra are shown in Figure 3d. Two emission bands were observed; the one at ca. 600 nm is assigned as the locally excited (LE)-state emission of the rhodamine unit, whereas the weak and broad band in the range of 690–800 nm in DCM is assigned to the CT emission [55]. No such CT emission band can be observed in other solvents, even in non-polar solvents. It is known that the CT state, especially the twisted CT state, is weakly emissive [56–58]. To the best of our knowledge, the emissive CT state of rhodamine was rarely reported. The CT emission observed for **RB-Pery** is unlikely due to the perylene unit; the CT state of perylene should be in a shorter wavelength range (ca. 600 nm, with phenothiazine as the electron donor). The emission wavelength should depend on the electron donor and the electronic coupling between the electron donor and acceptor [28]. The fluorescence excitation spectra for **RB-Pery** were compared with the UV-vis absorption spectra (Figure S7b,c). In *p*-XYL, the excitation spectrum shows a smaller magnitude compared to the UV-vis spectrum in the range of 370–460 nm, which indicates that there should be some other non-radiative decay channels. However, **RB-Pery** shows a noisy excitation spectrum in DCM due to the low fluorescence quantum yield (Figure S7c). In this case, the excitation spectrum gives a weak and distinct band in the 620–800 nm range, but such a band is absent in the absorption spectrum. This result indicates that the excitation in the range of 620–800 nm is more efficient to produce the CT excited state than that with excitation at the LE absorption band.

The luminescence lifetimes of the compounds in different solvents are presented in Table S2. The fluorescence of Pery shows monoexponential decaying kinetics; however, the fluorescence decay traces of **RB-Ph** and **RB-Pery** show different features. For instance, **RB-Ph** shows bi-exponential decay of the fluorescence in both *p*-XYL and TOL, but monoexponential decay in tetrahydrofuran (THF), DCM, and acetonitrile (ACN). For **RB-Pery**,

bi-exponential decay of the fluorescence was observed in all solvents, which indicates there are other emission decay channels besides the intrinsic emission of the chromophore unit, i.e., CT emission. We compiled the singlet oxygen ($^1\text{O}_2$) quantum yields of compounds determined in varying polarity solvents according to their E_T (30) values (Table S3). Pristine perylene exhibited a weak $^1\text{O}_2$ production ability, while no $^1\text{O}_2$ was observed for **RB-Ph**. The main dyad, **RB-Pery**, showed a low $^1\text{O}_2$ production ability (8.0% in *p*-XYL and 2.7% in TOL); this leads to ineffective SOCT-ISC in the dyad.

3.4. Cyclic Voltammograms of **RB-Ph** and **RB-Pery**

Cyclic voltammograms were recorded to study the electrochemical properties of the compounds (Figure 4). Similar to a previous report, only a single reversible oxidation wave at +0.61 V (vs. Fc/Fc^+) was observed in perylene and no reduction wave was observed up to the potential window used in the studies (Figure S9) [59]. For another reference, **RB-Ph**, reversible oxidation and reduction waves were observed at +0.89 V and -1.32 V, respectively (Table 2). For **RB-Pery**, two reversible oxidation waves at +0.58 V and +0.87 V and a reversible reduction wave at -1.29 V were observed. The first oxidation wave belongs to the perylene moiety, indicating that the perylene in the dyad is easy to oxidize. Therefore, perylene acts as an electron donor and the rhodamine unit acts as electron acceptor in **RB-Pery**.

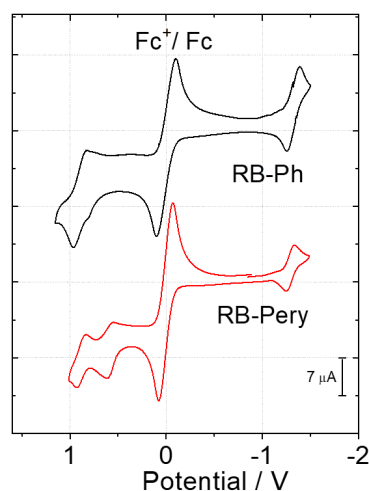


Figure 4. Cyclic voltammograms of **RB-Ph** and **RB-Pery** in deaerated DCM containing 0.10 M Bu_4NPF_6 as supporting electrolyte and Ag/AgNO_3 as reference electrode; redox potential is versus Fc/Fc^+ . Scan rates: 50 mV/s. $c = 1.0 \times 10^{-3}$ M; 25 °C.

Table 2. Electrochemical redox potentials of the compounds ^a.

Compounds	E_{OX} (V)	E_{RED} (V)
Pery	+0.61 ^b	– ^c
RB-Ph	+0.89	-1.32
RB-Pery	+0.58, +0.87	-1.29

^a Cyclic voltammetry in N_2 -saturated DCM containing a 0.10 M Bu_4NPF_6 , with Pt electrode as the counter electrode, glassy carbon electrode as the working electrode, and Ag/AgNO_3 couple as the reference electrode versus Fc/Fc^{2+} . ^b Literature value [59]. ^c Not observed.

3.5. Nanosecond Transient Absorption (ns-TA) Spectroscopy

In order to study the excited triplet-state formation, the nanosecond transient absorption (ns-TA) spectra of **RB-Pery** were recorded in solvents with different polarities. In DCM, a ground-state bleaching (GSB) band centred at ca. 565 nm was observed, which is due to the depletion of the ground state of the rhodamine moiety (Figure 5a). Interestingly, a broad excited-state absorption (ESA) band in the range of 450–550 nm was observed. The ns-TA of the triplet state of the rhodamine chromophore was studied previously [43,44,60], but very weak transient features in the range of 450–550 nm were observed. Instead, it was shown that

the triplet state of perylene shows a strong ESA band in this range [27,28,59,61]. Therefore, we propose that the triplet state in the dyad is not solely localized on the rhodamine unit. Contrarily, it is delocalized on both the xanthene chromophore and the perylene moiety, i.e., there is a triplet-state equilibrium. The T_1 energy of perylene is ca. 1.53 eV [61], and the T_1 state energy of the xanthene moiety is ca. 1.70 eV [43,44]; thus, triplet-state equilibrium between these comparatively close-lying triplet states at room temperature is anticipated.

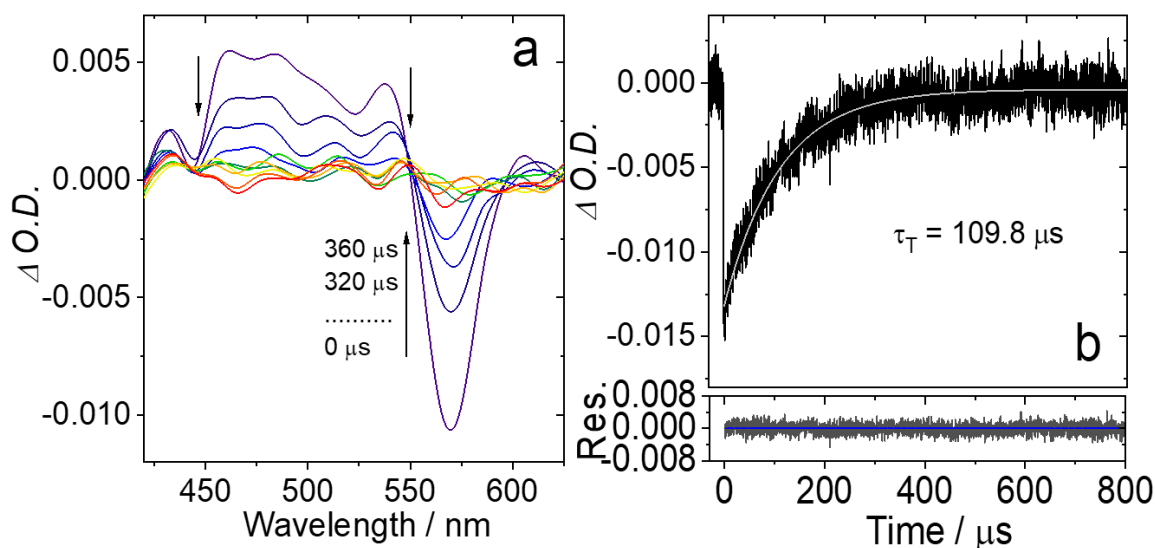


Figure 5. (a) Nanosecond transient absorption spectra of **RB-Pery** and (b) decay trace at 565 nm; $c = 2.0 \times 10^{-5}$ M in deaerated DCM. $\lambda_{\text{ex}} = 570$ nm; 25 °C.

The excited triplet-state lifetime of **RB-Pery** was determined as 109.8 μs in deaerated DCM (Figure 5b); however, when the solution was exposed to air, no transient signals were detected which proved the triplet state. Moreover, no transient signal was observed for **RB-Pery** in deaerated ACN. This highly solvent polarity-dependent triplet formation indicates the SOCT-ISC mechanism for triplet-state population in the dyad.

Previously, it was reported that the T_1 state of the rhodamine chromophore shows an absorption band at 420 nm [62], but later, it was proven that the neutral rhodamine radicals show similar absorption bands [63,64]. Upon the nanosecond pulsed laser excitation of native perylene, we detected a long-lived radical cation under both aerated/deaerated conditions (Figure S10). Such long-lived radical species were already reported for native perylene [31,65]. The proposed mechanism was a two-step (bi-photonic) process: firstly, the Pery singlet excited state is populated upon photoexcitation, which undergoes the triplet state, and then the triplet state is excited again to dissociate into ions by releasing/capturing solvated electrons [65]. For **RB-Pery**, we observed the long-lived rhodamine radical cation in solvents of *p*-XYL, TOL, and THF in both aerated/deaerated conditions (Figure S11). In this case, we assume the same mechanism for radical cation detection because the quenching of radical anion species with O_2 can be observed, whereas radical cations are insensitive to O_2 [66]. Moreover, it has been shown previously that rhodamine dye can form long-lived cation radicals (milliseconds) through photoionization in an aqueous solution, likely through both mono- and bi-photonic processes [67,68].

In another previous example, ns-TA spectra of rhodamine 6G radicals were found with the addition of an electron donor, *N,N*-diisopropylethylamine; the radical absorption band was observed at 421 nm (in DMSO) [64]. However, when we measured the ns-TA spectra of **RB-Pery** after adding triethylamine (TEA) or *N,N*-diisopropylethylamine, no signals were found. We further measured the ns-TA spectra of **RB-Pery** in a deaerated ACN solution and no transient signals were observed. Hence, we conducted the triplet-triplet energy transfer (TTET) experiment in this solvent from diiodo-BDP to **RB-Pery** to rationalize the triplet excited-state equilibrium (vide infra). For **RB-Ph**, no transient signals were

detected in all studied solvents. However, in DCM, the mixture of **RB-Ph** and TEA showed long-lived transient species of RB moieties with an ESA at 430 nm and GSB at 554 nm in the deaerated solution, which, upon exposure to air, quenched significantly (Figure S12).

These features are similar to the neutral rhodamine radicals [63,64]. This result also confirmed that the species observed in the case of **RB-Pery** in non-polar solvents is a cation radical, not a neutral radical. As stated above, rhodamine 6G can easily form a stable radical upon single-electron reduction [63,64]. Stable organic radicals are highly important for many research fields, such as molecular electronics, solar cells, organic light-emitting diodes, photoredox catalysis, and super-resolution microscopy [69–75].

To confirm the assignment of the ESA bands of the **RB-Pery** dyad, the intermolecular TTET from diiodo-BDP (Scheme 1) to the reference (**RB-Ph**, Pery) and **RB-Pery** was studied with ns-TA spectroscopy (Figures 6, 7 and S13). Upon 520 nm pulsed laser excitation, the mixture of diiodo-BDP/**RB-Ph** (Figure 6a,b) initially showed a different TA spectrum of diiodo-BDP (with a strong GSB band at 530 nm and weak ESA bands in the range of 400–780 nm), which diminished with delay times, and a new spectral feature developed. Note that the photoexcitation of **RB-Ph** alone does not show any transient signal. The decay trace of the mixture at 565 nm shows a rise phase at the early delay time and then decay at a longer delay time, which indicates the occurrence of TTET. The lifetime of the diiodo-BDP (energy donor) is reduced to 21.7 μs , which is much shorter than that of the pristine diiodo-BDP (99.5 μs , Figure S14), further verifying the TTET process. To better evaluate the transient species produced in the TTET experiment, global fitting of the ns-TA data was carried out, and species-associated difference spectra (SADSs) were obtained. The SADS of the $^3\text{RB}^*$ state (triplet lifetime of 277.8 μs) is obvious, with an ESA band in the range of 380–470 nm and a GSB band at around 550 nm. Moreover, this result further shows that the triplet energy of rhodamine is lower than 1.67 eV (~ 1.64 eV, predicted through TD-DFT), making TTET possible from the $^3\text{BDP}^*$ state ($E_{\text{T}1} = 1.67$ eV) [76].

By following the same protocol, the TTET experiment from diiodo-BDP to Pery ($E_{\text{T}1} = 1.53$ eV) was conducted (Figure 6c,d). In this case, new ESA bands in the range of 380–500 nm and a minor GSB at 430 nm developed, and the decay trace at 485 nm shows biphasic characteristics (simultaneous rise and decay), which indicates TTET manifestation. After global fitting, the first SADS shows a triplet state of $^3\text{BDP}^*$ ($\tau_{\text{T}} = 8.7$ μs) and the second SADS belongs to the $^3\text{Pery}^*$ ($\tau_{\text{T}} = 66.6$ μs).

Next, the TTET of the mixture of diiodo-BDP/**RB-Pery** was conducted under similar experimental conditions (Figure 7a,b). Note that **RB-Pery** alone does not give any transient signal upon excitation in ACN. Upon TTET, the GSB band of the energy donor, diiodo-BDP, quickly decreased, and a new GSB band at 565 nm developed, which is the GSB band of the rhodamine moiety. Moreover, the broad ESA band of the energy donor in the range of 380–460 nm transformed from one structureless band to a band with splitting peaks in the range of 380–510 nm. Note that this positive absorption band is different from the triplet absorption of **RB-Ph** and Pery alone obtained after TTET. In the first SADS, the species with a lifetime of 14 μs is the spectrum of the triplet energy donor. The red SADS with a lifetime of 142 μs can be assigned to the $\text{T}_1 \rightarrow \text{T}_n$ transient absorption of $^3\text{RB-Pery}^*$, which is similar to that observed upon direct photoexcitation (shown in Figure 5). Additionally, to allocate and analyse the observed triplet state in the **RB-Pery** dyad, we normalized the $^3\text{RB}^*$, $^3\text{Pery}^*$, and $^3[\text{RB-Pery}]^*$ states populated due to TTET in Figure 8a. The transient features of **RB-Pery** in the range of 380–510 nm resemble the ESA of pristine perylene, whereas the GSB is nearly similar to the **RB-Ph**. This result settled the argument that the triplet state in **RB-Pery** is delocalized on both moieties, which is further shown in the direct comparison of triplet features populated due to TTET and without TTET (Figure 8b). As mentioned above, the triplet energy of the perylene moiety is ~ 1.53 eV, and the rhodamine moiety is 1.64 eV (TD-DFT estimated), signifying the possibility of triplet energy balance/equilibrium between these two moieties in **RB-Pery** when measured in deaerated DCM. Previously, our group reported a delocalized triplet state in a bodipy–phenylethyl anthracene dyad; in that case, the triplet excited-state equilibrium was evident in the ns-TA spectra [77]. In the

present case, the triplet-state spin density of **RB-Pery** is delocalized on the whole molecule (Figure 1), which also supports triplet excited-state equilibrium.

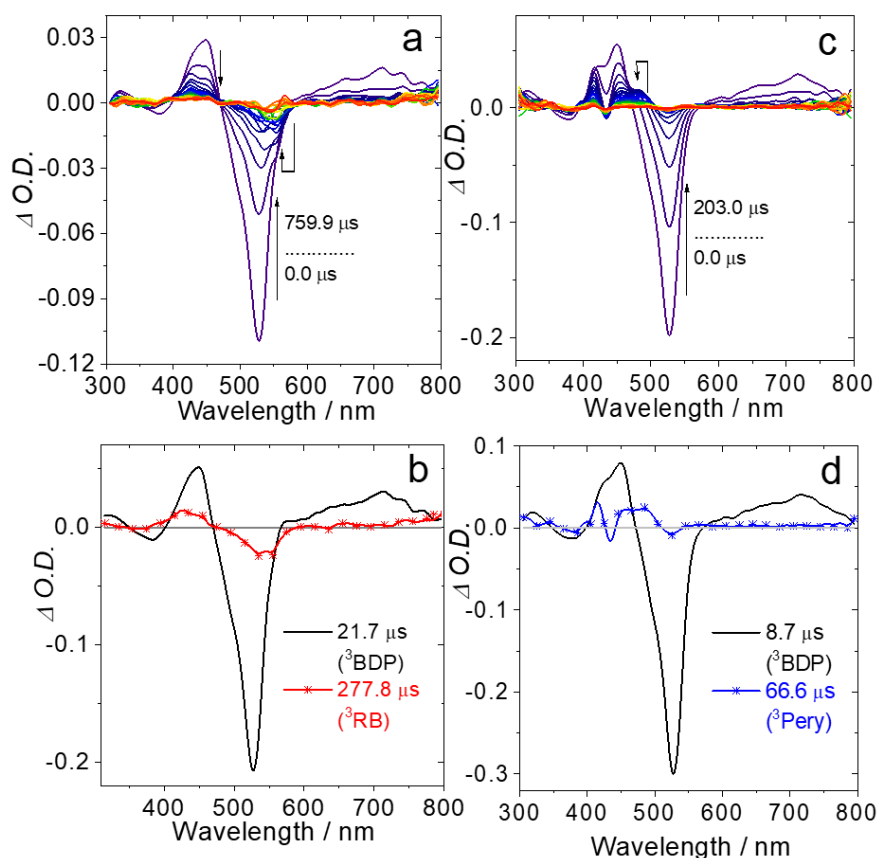


Figure 6. Intermolecular triplet–triplet energy transfer (TTET) from diiodo-BDP to different triplet energy acceptors, measured using ns-TA spectroscopy; (a) ns-TA spectra of a mixture of diiodo-BDP and **RB-Ph** and (b) SADS obtained after global analysis. (c) ns-TA spectra of the mixture of diiodo-BDP and Pery and (d) SADS obtained after global analysis. In all cases, the concentration of diiodo-BDP was fixed ($c[\text{diiodo-BDP}] = 5.0 \times 10^{-6} \text{ M}$) and 1:1 molar ratios of donor and acceptor were used. The selected kinetic traces of the TTET are supplied in the Supplementary Information. In deaerated ACN, $\lambda_{\text{ex}} = 520 \text{ nm}$; 25°C .

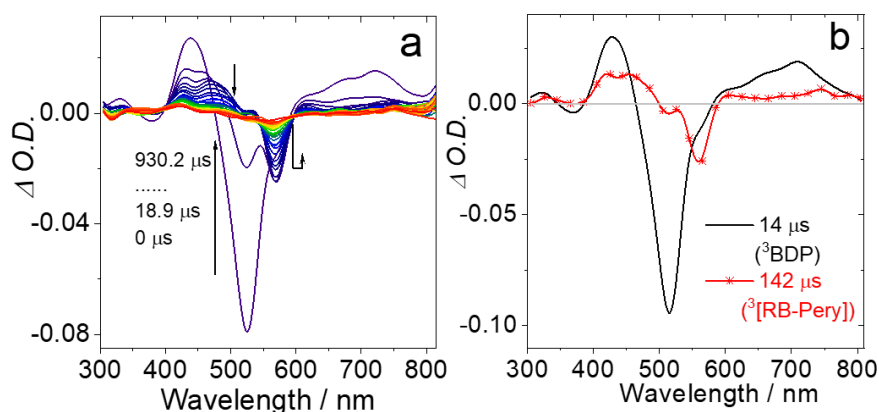


Figure 7. Intermolecular triplet–triplet energy transfer (TTET) from diiodo-BDP to **RB-Pery**, measured using ns-TA spectroscopy; (a) ns-TA spectra of a mixture of diiodo-BDP and **RB-Pery** and (b) SADS obtained after global analysis. The concentration of diiodo-BDP was fixed ($c[\text{diiodo-BDP}] = 5.0 \times 10^{-6} \text{ M}$) and 1:1 molar ratio of donor and acceptor was used. The selected kinetic traces of the TTET are supplied in the Supplementary Information. In deaerated ACN, $\lambda_{\text{ex}} = 520 \text{ nm}$; 25°C .

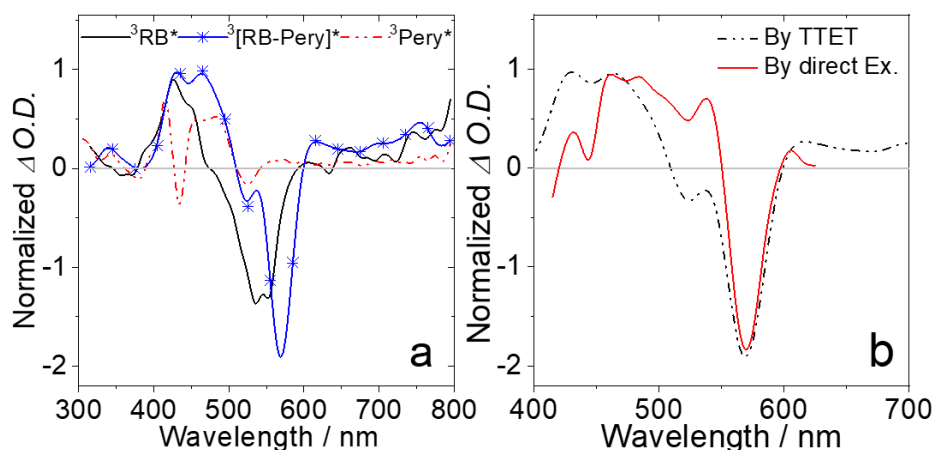
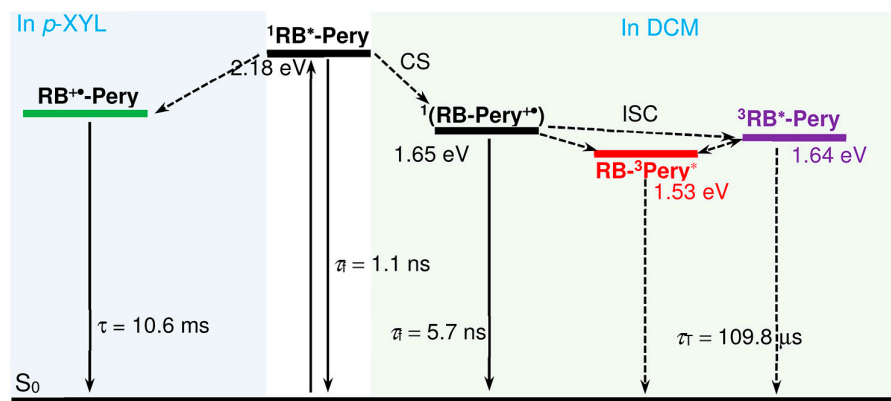


Figure 8. (a) Comparison of the normalized SADSs of ${}^3\text{RB}^*$, ${}^3\text{Pery}^*$, and ${}^3[\text{RB-Pery}]^*$ after TTET with 2,6-diiodo-BDP. (b) Normalized triplet-state spectra of **RB-Pery** upon direct photoexcitation and due to TTET with diiodo-BDP/**RB-Pery** mixture (the experimental spectrum was taken from Figure 5a).

To summarize the photophysical processes observed in the **RB-Pery** in different polarity solvents, we constructed a Jablonski diagram (Scheme 2). In DCM, upon the photoexcitation of the rhodamine moiety, the S_1 state of the rhodamine moiety was first populated. Subsequently, charge separation took place and gave a charge transfer state with an energy of 1.65 eV, supported by the CT emission band, followed by charge recombination results in SOCT-ISC, and a long-lived ($\tau_T = 109.8 \mu\text{s}$) delocalized triplet state was observed. As the perylene and rhodamine triplet-state energy difference is small ($\sim 0.11 \text{ eV}$), a triplet-state interconversion or triplet-state energy balance is possible. Resultantly, a delocalized triplet state was observed. On the other side, upon the photoexcitation of **RB-Pery** in non-polar solvents such as *p*-XYL or TOL, only a persistent rhodamine radical cation was detected (lifetime up to milliseconds).



Scheme 2. Simplified Jablonski diagram illustrating the photophysical processes of **RB-Pery** upon photoexcitation in different-polarity solvents: The energy level of ${}^1\text{RB}^*\text{-Pery}$ is calculated from the cross point of the normalized UV-vis absorption spectrum and normalized fluorescence emission spectrum in DCM. The energy level of ${}^1(\text{RB-Pery})^*$ is calculated based on the CT emission band, in DCM. The triplet excited-state energy level of $\text{RB-}{}^3\text{Pery}^*$ is based on literature values [61]. The triplet energy level of ${}^3\text{RB}^*\text{-Pery}$ is estimated through TD-DFT calculations of the rhodamine moiety at the B3LYP/6-31G level using Gaussian 09. *p*-XYL stands for *p*-xylene and DCM is dichloromethane.

4. Conclusions

In summary, a rhodamine (RB)-perylene (Pery) compact electron donor/acceptor dyad (**RB-Pery**) was synthesized and studied for the spin-orbit charge-transfer intersystem crossing (SOCT-ISC) mechanism. The steady-state UV-vis absorption spectra show negli-

gible electronic interaction between the perylene and the rhodamine units; however, the quenched emission of **RB-Pery** in polar solvents indicated photo-induced electron transfer. This is supported by the frontier molecular orbital calculations; HOMO is localized on the perylene unit and the LUMO is localized on the rhodamine unit. The nanosecond transient absorption (ns-TA) spectra of the dyad in DCM showed mixed characters of both the perylene and rhodamine triplet states. In fact, a delocalized triplet state was observed (i.e., the triplet states localized on the perylene and the rhodamine units are equilibrated); the triplet-state lifetime was determined as 109.8 μ s. Thus, the proposed photophysical processes of **RB-Pery** in deaerated DCM are as follows: $^1\text{RB}^*\text{-Pery} \rightarrow [\text{RB-Pery}^{+\bullet}] \rightarrow [^3\text{RB}^*\text{-Pery} \leftrightarrow \text{RB-}^3\text{Pery}^*]$. A long-lived rhodamine radical cation was observed in deaerated/aerated non-polar or low-polarity solvents (*p*-xylene or toluene), the lifetime of which is up to a millisecond time scale. The intermolecular triplet-triplet energy transfer, monitored using an ns-TA spectrometer, further verified the delocalized transient triplet features in the **RB-Pery** dyad. The potential energy curve (PEC) of the torsion between the electron donor and acceptor in the dyad indicates large rotation freedom in **RB-Pery**, and this may lead to inefficient SOCT-ISC and a low singlet-oxygen quantum yield (Φ_{Δ}) of only 8%. However, the lower torsional freedom can keep the geometry between the donor and acceptor in charge transport favourable manner and vertical configuration can enhance the ISC efficiency. Our results are also useful for both future SOCT-ISC studies and fundamental photochemistry studies.

Supplementary Materials: The following supporting information can be downloaded at: <https://www.mdpi.com/article/10.3390/photochem4010004/s1>, Figure S1: ^1H NMR spectrum of **RB-Ph** (CDCl_3 , 400 MHz); Figure S2: ^1H NMR spectrum of **RB-Pery** (CDCl_3 , 400 MHz); Figure S3: ^{13}C NMR spectrum of **RB-Ph** (CDCl_3 , 126 MHz); Figure S4: ^{13}C NMR spectrum of **RB-Pery** (CDCl_3 , 126 MHz); Figure S5: ESI-HRMS of **RB-Pery**; Figure S6: UV-vis absorption spectra of compound (a) **RB-Ph** and (b) **RB-Pery** in different solvents. $c = 1.0 \times 10^{-5}$ M; Figure S7: (a) Fluorescence emission spectra (optically-matched solutions were used, $A = 0.10$) of **RB-Pery** in different polarity solvents, $\lambda_{\text{ex}} = 415$ nm. Normalized UV-vis absorption and fluorescence excitation spectra of **RB-Pery** (b) in *p*-XYL monitored at 650 nm and (c) in DCM monitored at 800 nm. $c \approx 1.0 \times 10^{-5}$ M. 25 $^{\circ}\text{C}$; Figure S8: Fluorescence decay traces of the compounds in different solvents (a) **RB-Pery** monitored at 585 nm and (b) **RB-Ph** monitored at 585 nm. Fluorescence decay trace of the **RB-Pery** in DCM (c) monitored at 630 nm and (d) monitored at 690 nm. Excited with a 405 nm picosecond pulsed laser. $c \approx 1.0 \times 10^{-5}$ M. 25 $^{\circ}\text{C}$; Figure S9: Cyclic voltammogram of perylene. Conditions: in deaerated DCM containing 0.10 M Bu_4NPF_6 as supporting electrode, Ag/AgNO_3 as reference electrode, redox potentials are *versus* Fc/Fc^+ . Scan rates: 50 mV/s. $c = 1.0 \times 10^{-3}$ M. 25 $^{\circ}\text{C}$; Figure S10: (a) Transient absorption spectra of Pery in deaerated DCM and (b) decay traces at 540 nm in DCM, $c = 2.0 \times 10^{-5}$ M, $\lambda_{\text{ex}} = 432$ nm. 25 $^{\circ}\text{C}$; Figure S11: Transient absorption spectra of **RB-Pery**, (a) in deaerated *p*-XYL, $c = 1.0 \times 10^{-5}$ M; (b) in deaerated TOL, $c = 1.0 \times 10^{-5}$ M; (c) in deaerated THF, $c = 2.0 \times 10^{-5}$ M; (d-f) respective decay traces at 575 nm under aerated and deaerated conditions. $\lambda_{\text{ex}} = 570$ nm. 25 $^{\circ}\text{C}$; Figure S12: Transient absorption spectra of **RB-Ph** ($c = 1.0 \times 10^{-4}$ M) upon adding TEA ($c = 4.0 \times 10^{-3}$ M) (a) in deaerated DCM, (b) in aerated DCM and (c) decay traces at 560 nm in both cases. $\lambda_{\text{ex}} = 550$ nm. 25 $^{\circ}\text{C}$; Figure S13: Intermolecular triplet-triplet energy transfer (TTET): from diiodo-BDP to **RB-Ph**, **Pery** and **RB-Pery** measured by ns-TA spectroscopy; (a) selected kinetic traces of the mixture of the ns-TA spectra of diiodo-BDP and **RB-Ph**. (b) selected kinetic traces of the mixture of the ns-TA spectra of diiodo-BDP and Pery. (c) selected kinetic traces of the mixture of the ns-TA spectra of diiodo-BDP and **RB-Pery**. The concentration of diiodo-BDP was fixed $c[\text{diiodo-BDP}] = 5.0 \times 10^{-6}$ M and 1:1 molar ratios were used in every case. The ns-TA spectra are given in the main text. In deaerated ACN, $\lambda_{\text{ex}} = 520$ nm. 25 $^{\circ}\text{C}$; Figure S14: (a) Nanosecond transient absorption spectra of diiodo-BDP and (b) decay trace at 530 nm; $c = 5.0 \times 10^{-6}$ M in deaerated ACN. $\lambda_{\text{ex}} = 520$ nm. 25 $^{\circ}\text{C}$; Figure S15: Selected kinetic decay traces obtained after global fitting analysis (a) from ns-TA data of diiodo-BDP/**RB-Ph** mixture (b) from ns-TA data of diiodo-BDP/Pery mixture and (c) from ns-TA data of diiodo-BDP/**RB-Pery**. The respective raw data and SADS spectra are given in the main text Figures 6 and 7; Table S1: Absolute Photo-luminescence Quantum Yield of the Compounds in different solvents; Table S2: Luminescence Lifetime of the Compounds in different solvents; Table S3: Singlet Oxygen Quantum Yields of Compounds in Different Solvents.

Author Contributions: Conceptualization, J.Z.; methodology, M.I., D.L. and K.Y.; writing—original draft preparation, J.Z., M.I. and X.Z.; supervision, J.Z. All authors have read and agreed to the published version of the manuscript.

Funding: We thank the Ministry of Science and Technology (2023YFE0197600), the NSFC (U2001222), the Research and Innovation Team Project of the Dalian University of Technology (DUT2022TB10), the Fundamental Research Funds for the Central Universities (DUT22LAB610), and the State Key Laboratory of Fine Chemicals for financial support.

Data Availability Statement: The original data of this work can be requested from the corresponding author.

Conflicts of Interest: The authors declare no conflicts of interest.

References

1. Khramov, D.M.; Boydston, A.J.; Bielawski, C.W. Synthesis and Study of Janus Bis(carbene)s and Their Transition-Metal Complexes. *Angew. Chem. Int. Ed.* **2006**, *45*, 6186–6189. [[CrossRef](#)]
2. Wang, X.; Goeb, S.; Ji, Z.; Pogulaichenko, N.A.; Castellano, F.N. Homogeneous Photocatalytic Hydrogen Production Using π -Conjugated Platinum(II) Arylacetylide Sensitizers. *Inorg. Chem.* **2011**, *50*, 705–707. [[CrossRef](#)]
3. Zhao, J.; Wu, W.; Sun, J.; Guo, S. Triplet photosensitizers: From molecular design to applications. *Chem. Soc. Rev.* **2013**, *42*, 5323–5351. [[CrossRef](#)]
4. Zhao, J.; Xu, K.; Yang, W.; Wang, Z.; Zhong, F. The triplet excited state of Bodipy: Formation, modulation and application. *Chem. Soc. Rev.* **2015**, *44*, 8904–8939. [[CrossRef](#)]
5. Zhou, G.-J.; Wong, W.-Y. Organometallic acetylides of Pt^{II}, Au^I and Hg^{II} as new generation optical power limiting materials. *Chem. Soc. Rev.* **2011**, *40*, 2541–2566. [[CrossRef](#)]
6. Zhao, Q.; Li, F.; Huang, C. Phosphorescent chemosensors based on heavy-metal complexes. *Chem. Soc. Rev.* **2010**, *39*, 3007–3030. [[CrossRef](#)]
7. Ji, S.; Wu, W.; Wu, W.; Guo, H.; Zhao, J. Ruthenium(II) Polyimine Complexes with a Long-Lived ³IL Excited State or a ³MLCT/³IL Equilibrium: Efficient Triplet Sensitizers for Low-Power Upconversion. *Angew. Chem. Int. Ed.* **2011**, *50*, 1626–1629. [[CrossRef](#)] [[PubMed](#)]
8. Wang, Z.; Zhao, J.; Barbon, A.; Toffoletti, A.; Liu, Y.; An, Y.; Xu, L.; Karatay, A.; Yaglioglu, H.G.; Yildiz, E.A.; et al. Radical-Enhanced Intersystem Crossing in New Bodipy Derivatives and Application for Efficient Triplet–Triplet Annihilation Upconversion. *J. Am. Chem. Soc.* **2017**, *139*, 7831–7842. [[CrossRef](#)] [[PubMed](#)]
9. Chi, Y.; Chou, P.-T. Contemporary progresses on neutral, highly emissive Os(II) and Ru(II) complexes. *Chem. Soc. Rev.* **2007**, *36*, 1421–1431. [[CrossRef](#)] [[PubMed](#)]
10. Fernández-Moreira, V.; Thorp-Greenwood, F.L.; Coogan, M.P. Application of d⁶ transition metal complexes in fluorescence cell imaging. *Chem. Commun.* **2010**, *46*, 186–202. [[CrossRef](#)] [[PubMed](#)]
11. Herberger, J.; Winter, R.F. Platinum emitters with dye-based σ -aryl ligands. *Coord. Chem. Rev.* **2019**, *400*, 213048. [[CrossRef](#)]
12. Ziessel, R.; Allen, B.D.; Rewinska, D.B.; Harriman, A. Selective Triplet-State Formation during Charge Recombination in a Fullerene/Bodipy Molecular Dyad (Bodipy=Borondipyromethene). *Chem.—Eur. J.* **2009**, *15*, 7382–7393. [[CrossRef](#)] [[PubMed](#)]
13. Amin, A.N.; El-Khouly, M.E.; Subbaiyan, N.K.; Zandler, M.E.; Fukuzumi, S.; D’Souza, F. A novel BF₂-chelated azadipyromethene–fullerene dyad: Synthesis, electrochemistry and photodynamics. *Chem. Commun.* **2012**, *48*, 206–208. [[CrossRef](#)] [[PubMed](#)]
14. Huang, L.; Yu, X.; Wu, W.; Zhao, J. Styryl Bodipy-C₆₀ Dyads as Efficient Heavy-Atom-Free Organic Triplet Photosensitizers. *Org. Lett.* **2012**, *14*, 2594–2597. [[CrossRef](#)]
15. Wu, Y.; Liu, K.; Liu, H.; Zhang, Y.; Zhang, H.; Yao, J.; Fu, H. Impact of Intermolecular Distance on Singlet Fission in a Series of TIPS Pentacene Compounds. *J. Phys. Chem. Lett.* **2014**, *5*, 3451–3455. [[CrossRef](#)] [[PubMed](#)]
16. Zhang, Y.-D.; Wu, Y.; Xu, Y.; Wang, Q.; Liu, K.; Chen, J.-W.; Cao, J.-J.; Zhang, C.; Fu, H.; Zhang, H.-L. Excessive Exoergicity Reduces Singlet Exciton Fission Efficiency of Heteroacenes in Solutions. *J. Am. Chem. Soc.* **2016**, *138*, 6739–6745. [[CrossRef](#)]
17. Bröring, M.; Krüger, R.; Link, S.; Kleeberg, C.; Köhler, S.; Xie, X.; Ventura, B.; Flamigni, L. Bis(BF₂)-2,2′-Bidipyrrins (BisBODIPYs): Highly Fluorescent BODIPY Dimers with Large Stokes Shifts. *Chem.—Eur. J.* **2008**, *14*, 2976–2983. [[CrossRef](#)]
18. Hussain, M.; Taddei, M.; Bussotti, L.; Foggi, P.; Zhao, J.; Liu, Q.; Di Donato, M. Intersystem Crossing in Naphthalenediimide–Oxoverdazyl Dyads: Synthesis and Study of the Photophysical Properties. *Chem.—Eur. J.* **2019**, *25*, 15615–15627. [[CrossRef](#)]
19. Dance, Z.E.X.; Mi, Q.; McCamant, D.W.; Ahrens, M.J.; Ratner, M.A.; Wasielewski, M.R. Time-Resolved EPR Studies of Photogenerated Radical Ion Pairs Separated by p-Phenylene Oligomers and of Triplet States Resulting from Charge Recombination. *J. Phys. Chem. B* **2006**, *110*, 25163–25173. [[CrossRef](#)]
20. Colvin, M.T.; Ricks, A.B.; Scott, A.M.; Smeigh, A.L.; Carmieli, R.; Miura, T.; Wasielewski, M.R. Magnetic Field-Induced Switching of the Radical-Pair Intersystem Crossing Mechanism in a Donor–Bridge–Acceptor Molecule for Artificial Photosynthesis. *J. Am. Chem. Soc.* **2011**, *133*, 1240–1243. [[CrossRef](#)]
21. Kasha, M.; Rawls, H.R.; El-Bayoumi, M.A. The Exciton Model in Molecular Spectroscopy. *Pure Appl. Chem.* **1965**, *11*, 371–392. [[CrossRef](#)]

22. Weiss, E.A.; Ahrens, M.J.; Sinks, L.E.; Ratner, M.A.; Wasielewski, M.R. Solvent Control of Spin-Dependent Charge Recombination Mechanisms within Donor–Conjugated Bridge–Acceptor Molecules. *J. Am. Chem. Soc.* **2004**, *126*, 9510–9511. [[CrossRef](#)] [[PubMed](#)]
23. Buck, J.T.; Boudreau, A.M.; DeCarminé, A.; Wilson, R.W.; Hampsey, J.; Mani, T. Spin-Allowed Transitions Control the Formation of Triplet Excited States in Orthogonal Donor–Acceptor Dyads. *Chem* **2019**, *5*, 138–155. [[CrossRef](#)]
24. Wang, Z.; Zhao, J. Bodipy–Anthracene Dyads as Triplet Photosensitizers: Effect of Chromophore Orientation on Triplet-State Formation Efficiency and Application in Triplet–Triplet Annihilation Upconversion. *Org. Lett.* **2017**, *19*, 4492–4495. [[CrossRef](#)] [[PubMed](#)]
25. Hou, Y.; Biskup, T.; Rein, S.; Wang, Z.; Bussotti, L.; Russo, N.; Foggi, P.; Zhao, J.; Di Donato, M.; Mazzone, G.; et al. Spin–Orbit Charge Recombination Intersystem Crossing in Phenothiazine–Anthracene Compact Dyads: Effect of Molecular Conformation on Electronic Coupling, Electronic Transitions, and Electron Spin Polarizations of the Triplet States. *J. Phys. Chem. C* **2018**, *122*, 27850–27865. [[CrossRef](#)]
26. Chen, K.; Yang, W.; Wang, Z.; Iagatti, A.; Bussotti, L.; Foggi, P.; Ji, W.; Zhao, J.; Di Donato, M. Triplet Excited State of BODIPY Accessed by Charge Recombination and Its Application in Triplet–Triplet Annihilation Upconversion. *J. Phys. Chem. A* **2017**, *121*, 7550–7564. [[CrossRef](#)]
27. Wang, Z.; Ivanov, M.; Gao, Y.; Bussotti, L.; Foggi, P.; Zhang, H.; Russo, N.; Dick, B.; Zhao, J.; Di Donato, M.; et al. Spin–Orbit Charge-Transfer Intersystem Crossing (ISC) in Compact Electron Donor–Acceptor Dyads: ISC Mechanism and Application as Novel and Potent Photodynamic Therapy Reagents. *Chem.—Eur. J.* **2020**, *26*, 1091–1102. [[CrossRef](#)]
28. Imran, M.; Sukhanov, A.A.; Wang, Z.; Karatay, A.; Zhao, J.; Mahmood, Z.; Elmali, A.; Voronkova, V.K.; Hayvali, M.; Xing, Y.H.; et al. Electronic Coupling and Spin–Orbit Charge-Transfer Intersystem Crossing in Phenothiazine–Perylene Compact Electron Donor/Acceptor Dyads. *J. Phys. Chem. C* **2019**, *123*, 7010–7024. [[CrossRef](#)]
29. Zhao, Y.; Duan, R.; Zhao, J.; Li, C. Spin–Orbit Charge Transfer Intersystem Crossing in Perylenemonoimide–Phenothiazine Compact Electron Donor–Acceptor Dyads. *Chem. Commun.* **2018**, *54*, 12329–12332. [[CrossRef](#)]
30. Zhang, X.; Elmali, A.; Duan, R.; Liu, Q.; Ji, W.; Zhao, J.; Li, C.; Karatay, A. Charge Separation, Recombination and Intersystem Crossing of Directly Connected Perylenemonoimide–Carbazole Electron Donor/Acceptor Dyads. *Phys. Chem. Chem. Phys.* **2020**, *22*, 6376–6390. [[CrossRef](#)]
31. Imran, M.; El-Zohry, A.M.; Matt, C.; Taddei, M.; Doria, S.; Bussotti, L.; Foggi, P.; Zhao, J.; Di Donato, M.; Mohammed, O.F.; et al. Intersystem Crossing via Charge Recombination in a Perylene–Naphthalimide Compact Electron Donor/Acceptor Dyad. *J. Mater. Chem. C* **2020**, *8*, 8305–8319. [[CrossRef](#)]
32. Filatov, M.A. Heavy-atom-free BODIPY Photosensitizers with Intersystem Crossing Mediated by Intramolecular Photoinduced Electron Transfer. *Org. Biomol. Chem.* **2020**, *18*, 10–27. [[CrossRef](#)]
33. Gibbons, D.J.; Farawar, A.; Mazzella, P.; Leroy-Lhez, S.; Williams, R.M. Making Triplets from Photo-Generated Charges: Observations, Mechanisms and Theory. *Photochem. Photobiol. Sci.* **2020**, *19*, 136–158. [[CrossRef](#)] [[PubMed](#)]
34. Zhang, X.; Wang, Z.; Hou, Y.; Yan, Y.; Zhao, J.; Dick, B. Recent Development of Heavy-Atom-Free Triplet Photosensitizers: Molecular Structure Design, Photophysics and Application. *J. Mater. Chem. C* **2021**, *9*, 11944–11973. [[CrossRef](#)]
35. He, G.; Guo, D.; He, C.; Zhang, X.; Zhao, X.; Duan, C. A Color-Tunable Europium Complex Emitting Three Primary Colors and White Light. *Angew. Chem. Int. Ed.* **2009**, *48*, 6132–6135. [[CrossRef](#)] [[PubMed](#)]
36. Lin, W.; Yuan, L.; Cao, Z.; Feng, Y.; Song, J. Through-Bond Energy Transfer Cassettes with Minimal Spectral Overlap between the Donor Emission and Acceptor Absorption: Coumarin–Rhodamine Dyads with Large Pseudo-Stokes Shifts and Emission Shifts. *Angew. Chem. Int. Ed.* **2010**, *49*, 375–379. [[CrossRef](#)]
37. Belov, V.N.; Wurm, C.A.; Boyarskiy, V.P.; Jakobs, S.; Hell, S.W. Rhodamines NN: A Novel Class of Caged Fluorescent Dyes. *Angew. Chem. Int. Ed.* **2010**, *49*, 3520–3523. [[CrossRef](#)] [[PubMed](#)]
38. Krishnamoorthy, K.; Begley, T.P. Reagent for the Detection of Protein Thiocarboxylates in the Bacterial Proteome: Lissamine Rhodamine B Sulfonyl Azide. *J. Am. Chem. Soc.* **2010**, *132*, 11608–11612. [[CrossRef](#)]
39. Koide, Y.; Urano, Y.; Hanaoka, K.; Terai, T.; Nagano, T. Development of an Si-Rhodamine-Based Far-Red to Near-Infrared Fluorescence Probe Selective for Hypochlorous Acid and Its Applications for Biological Imaging. *J. Am. Chem. Soc.* **2011**, *133*, 5680–5682. [[CrossRef](#)]
40. Hu, L.; Pei, C.; Li, Z.; Wang, C.; Yang, G.; Sun, W. Synthesis and Photophysics of a Broadband Absorbing Texaphyrin Derivative Bearing a Rhodamine 6G Motif. *Org. Chem. Front.* **2014**, *1*, 506–514. [[CrossRef](#)]
41. Majumdar, P.; Cui, X.; Xu, K.; Zhao, J. Switching of the Photophysical Properties of Bodipy-Derived trans Bis(tributylphosphine) Pt(II) Bisacetylde Complexes with Rhodamine as the Acid-Activatable Unit. *Dalton Trans.* **2015**, *44*, 4032–4045. [[CrossRef](#)] [[PubMed](#)]
42. Cheng, Y.; Li, L.; Wei, F.; Wong, K.M.-C. Alkynylplatinum(II) Terpyridine System Coupled with Rhodamine Derivative: Interplay of Aggregation, Deaggregation, and Ring-Opening Processes for Ratiometric Luminescence Sensing. *Inorg. Chem.* **2018**, *57*, 6439–6446. [[CrossRef](#)] [[PubMed](#)]
43. Huang, L.; Zeng, L.; Guo, H.; Wu, W.; Wu, W.; Ji, S.; Zhao, J. Room-Temperature Long-Lived ³IL Excited State of Rhodamine in an NN Pt^{II} Bis(acetylde) Complex with Intense Visible-Light Absorption. *Eur. J. Inorg. Chem.* **2011**, *2011*, 4527–4533. [[CrossRef](#)]
44. Liu, C.; Zhou, L.; Wei, F.; Li, L.; Zhao, S.; Gong, P.; Cai, L.; Wong, K.M.-C. Versatile Strategy To Generate a Rhodamine Triplet State as Mitochondria-Targeting Visible-Light Photosensitizers for Efficient Photodynamic Therapy. *ACS Appl. Mater. Interfaces* **2019**, *11*, 8797–8806. [[CrossRef](#)]

45. Yang, H.; Han, C.; Zhu, X.; Liu, Y.; Zhang, K.Y.; Liu, S.; Zhao, Q.; Li, F.; Huang, W. Upconversion Luminescent Chemodosimeter Based on NIR Organic Dye for Monitoring Methylmercury In Vivo. *Adv. Funct. Mater.* **2016**, *26*, 1945–1953. [[CrossRef](#)]
46. Tian, R.; Sun, W.; Li, M.; Long, S.; Li, M.; Fan, J.; Guo, L.; Peng, X. Development of a Novel Anti-tumor Theranostic Platform: A Near-Infrared Molecular Upconversion Sensitizer for Deep-Seated Cancer Photodynamic Therapy. *Chem. Sci.* **2019**, *10*, 10106–10112. [[CrossRef](#)]
47. Wan, W.; Li, A.D.Q. Discovery of a New Light–Molecule Interaction: Supracence Reveals What Is Missing in Fluorescence Imaging. *Angew. Chem. Int. Ed.* **2019**, *58*, 13739–13743. [[CrossRef](#)]
48. Frisch, M.J.; Trucks, G.W.; Schlegel, H.B.; Scuseria, G.E.; Robb, M.A.; Cheeseman, J.R.; Scalmani, G.; Barone, V.; Petersson, G.A.; Nakatsuji, H.; et al. *Gaussian 09W, Revision E.01*; Gaussian Inc.: Wallingford, CT, USA, 2009.
49. Liu, D.; El-Zohry, A.M.; Taddei, M.; Matt, C.; Bussotti, L.; Wang, Z.; Zhao, J.; Mohammed, O.F.; Di Donato, M.; Weber, S. Long-Lived Charge-Transfer State Induced by Spin-Orbit Charge Transfer Intersystem Crossing (SOCT–ISC) in a Compact Spiro Electron Donor/Acceptor Dyad. *Angew. Chem. Int. Ed.* **2020**, *59*, 11591–11599. [[CrossRef](#)]
50. Hu, M.; Sukhanov, A.A.; Zhang, X.; Elmali, A.; Zhao, J.; Ji, S.; Karatay, A.; Voronkova, V.K. Spiro Rhodamine–Perylene Compact Electron Donor–Acceptor Dyads: Conformation Restriction, Charge Separation, and Spin–Orbit Charge Transfer Intersystem Crossing. *J. Phys. Chem. B* **2021**, *125*, 4187–4203. [[CrossRef](#)]
51. Filatov, M.A.; Karuthedath, S.; Polestshuk, P.M.; Callaghan, S.; Flanagan, K.J.; Wiesner, T.; Laquai, F.; Senge, M.O. BODIPY–Pyrene and Perylene Dyads as Heavy-Atom-Free Singlet Oxygen Sensitizers. *ChemPhotoChem* **2018**, *2*, 606–615. [[CrossRef](#)]
52. Dance, Z.E.X.; Mickley, S.M.; Wilson, T.M.; Ricks, A.B.; Scott, A.M.; Ratner, M.A.; Wasielewski, M.R. Intersystem Crossing Mediated by Photoinduced Intramolecular Charge Transfer: Julolidine–Anthracene Molecules with Perpendicular π Systems. *J. Phys. Chem. A* **2008**, *112*, 4194–4201. [[CrossRef](#)]
53. Zhang, X.-F.; Feng, N. Photoinduced Electron Transfer-based Halogen-free Photosensitizers: Covalent meso-Aryl (Phenyl, Naphthyl, Anthryl, and Pyrenyl) as Electron Donors to Effectively Induce the Formation of the Excited Triplet State and Singlet Oxygen for BODIPY Compounds. *Chem.—Asian J.* **2017**, *12*, 2447–2456. [[CrossRef](#)]
54. Wang, Z.; Sukhanov, A.A.; Toffoletti, A.; Sadiq, F.; Zhao, J.; Barbon, A.; Voronkova, V.K.; Dick, B. Insights into the Efficient Intersystem Crossing of Bodipy–Anthracene Compact Dyads with Steady-State and Time-Resolved Optical/Magnetic Spectroscopies and Observation of the Delayed Fluorescence. *J. Phys. Chem. C* **2019**, *123*, 265–274. [[CrossRef](#)]
55. Ganesan, P.; Baggerman, J.; Zhang, H.; Sudhölter, E.J.R.; Zuilhof, H. Femtosecond Time-Resolved Photophysics of 1,4,5,8-Naphthalene Diimides. *J. Phys. Chem. A* **2007**, *111*, 6151–6156. [[CrossRef](#)]
56. Arbeloa, F.L.; Arbeloa, T.L.; Bartolomé, P.H.; Estévez, M.J.T.; Arbeloa, I.L. TICT and ULM models for the Radiationless Deactivation of Rhodamines. *Proc. Indian Acad. Sci. (Chem. Sci.)* **1992**, *104*, 165–171. [[CrossRef](#)]
57. Liu, X.; Qiao, Q.; Tian, W.; Liu, W.; Chen, J.; Lang, M.J.; Xu, Z. Aziridinyl Fluorophores Demonstrate Bright Fluorescence and Superior Photostability by Effectively Inhibiting Twisted Intramolecular Charge Transfer. *J. Am. Chem. Soc.* **2016**, *138*, 6960–6963. [[CrossRef](#)] [[PubMed](#)]
58. Lv, X.; Gao, C.; Han, T.; Shi, H.; Guo, W. Improving the Quantum Yields of Fluorophores by Inhibiting Twisted Intramolecular Charge Transfer Using Electron-Withdrawing Group-Functionalized Piperidine Auxochromes. *Chem. Commun.* **2020**, *56*, 715–718. [[CrossRef](#)] [[PubMed](#)]
59. Xu, K.; Zhao, J.; Moore, E.G. Covalently Bonded Perylene–DiiodoBodipy Dyads for Thiol-Activatable Triplet–Triplet Annihilation Upconversion. *J. Phys. Chem. C* **2017**, *121*, 22665–22679. [[CrossRef](#)]
60. Li, G.; Mark, M.F.; Lv, H.; McCamant, D.W.; Eisenberg, R. Rhodamine–Platinum Diimine Dithiolate Complex Dyads as Efficient and Robust Photosensitizers for Light-Driven Aqueous Proton Reduction to Hydrogen. *J. Am. Chem. Soc.* **2018**, *140*, 2575–2586. [[CrossRef](#)]
61. Cui, X.; El-Zohry, A.M.; Wang, Z.; Zhao, J.; Mohammed, O.F. Homo- or Hetero-Triplet–Triplet Annihilation? A Case Study with Perylene–BODIPY Dyads/Triads. *J. Phys. Chem. C* **2017**, *121*, 16182–16192. [[CrossRef](#)]
62. Beaumont, P.C.; Johnson, D.G.; Parsons, B.J. Excited State and Free Radical Properties of Rhodamine Dyes in Aqueous Solution: A Laser Flash Photolysis and Pulse Radiolysis Study. *J. Photochem. Photobiol. A* **1997**, *107*, 175–183. [[CrossRef](#)]
63. van de Linde, S.; Krstić, I.; Prisner, T.; Doose, S.; Heilemann, M.; Sauer, M. Photoinduced Formation of Reversible Dye Radicals and Their Impact on Super-Resolution Imaging. *Photochem. Photobiol. Sci.* **2011**, *10*, 499–506. [[CrossRef](#)]
64. Slanina, T.; Oberschmid, T. Rhodamine 6G Radical: A Spectro (Fluoro) Electrochemical and Transient Spectroscopic Study. *ChemCatChem* **2018**, *10*, 4182–4190. [[CrossRef](#)]
65. Kawai, K.; Yamamoto, N.; Tsubomura, H. Simultaneous Formation of Perylene Cation and Anion by Flash Excitation of Perylene in Solutions. *Bull. Chem. Soc. Jpn.* **1970**, *43*, 2266–2268. [[CrossRef](#)]
66. Kabe, R.; Adachi, C. Organic long persistent luminescence. *Nature* **2017**, *550*, 384–387. [[CrossRef](#)] [[PubMed](#)]
67. Ferguson, M.W.; Beaumont, P.C.; Jones, S.E.; Navaratnam, S.; Parsons, B.J. Excited state and free radical properties of Rhodamine 123: A laser flash photolysis and radiolysis study. *Phys. Chem. Chem. Phys.* **1999**, *1*, 261–268. [[CrossRef](#)]
68. Navaratnam, S.; Parsons, B.J. Kinetic and spectral properties of rhodamine 6G free radicals: A pulse radiolysis study. *J. Photochem. Photobiol. A* **2002**, *153*, 153–162. [[CrossRef](#)]
69. Zhang, Z.; Chen, P.; Murakami, T.N.; Zakeeruddin, S.M.; Grätzel, M. The 2,2,6,6-Tetramethyl-1-piperidinyloxy Radical: An Efficient, Iodine-Free Redox Mediator for Dye-Sensitized Solar Cells. *Adv. Funct. Mater.* **2008**, *18*, 341–346. [[CrossRef](#)]

70. Heilemann, M.; van de Linde, S.; Mukherjee, A.; Sauer, M. Super-Resolution Imaging with Small Organic Fluorophores. *Angew. Chem. Int. Ed.* **2009**, *48*, 6903–6908. [[CrossRef](#)] [[PubMed](#)]
71. van de Linde, S.; Löschberger, A.; Klein, T.; Heidebreder, M.; Wolter, S.; Heilemann, M.; Sauer, M. Direct stochastic optical reconstruction microscopy with standard fluorescent probes. *Nat. Protoc.* **2011**, *6*, 991–1009. [[CrossRef](#)]
72. Frisenda, R.; Gaudenzi, R.; Franco, C.; Mas-Torrent, M.; Rovira, C.; Veciana, J.; Alcon, I.; Bromley, S.T.; Burzurí, E.; van der Zant, H.S.J. Kondo Effect in a Neutral and Stable All Organic Radical Single Molecule Break Junction. *Nano Lett.* **2015**, *15*, 3109–3114. [[CrossRef](#)]
73. Peng, Q.; Obolda, A.; Zhang, M.; Li, F. Organic Light-Emitting Diodes Using a Neutral π Radical as Emitter: The Emission from a Doublet. *Angew. Chem. Int. Ed.* **2015**, *54*, 7091–7095. [[CrossRef](#)] [[PubMed](#)]
74. Ghosh, I.; König, B. Chromoselective Photocatalysis: Controlled Bond Activation through Light-Color Regulation of Redox Potentials. *Angew. Chem. Int. Ed.* **2016**, *55*, 7676–7679. [[CrossRef](#)] [[PubMed](#)]
75. Romero, N.A.; Nicewicz, D.A. Organic Photoredox Catalysis. *Chem. Rev.* **2016**, *116*, 10075–10166. [[CrossRef](#)] [[PubMed](#)]
76. Liu, D.; Zhao, Y.; Wang, Z.; Xu, K.; Zhao, J. Exploiting the Benefit of $S_0 \rightarrow T_1$ Excitation in Triplet–Triplet Annihilation Upconversion to Attain Large Anti-Stokes Shifts: Tuning the Triplet State Lifetime of a Tris(2,2'-bipyridine) Osmium(II) Complex. *Dalton Trans.* **2018**, *47*, 8619–8628. [[CrossRef](#)]
77. Lei, Y.; Chen, K.; Tang, G.; Zhao, J.; Gurzadyan, G.G. Bodipy-Phenylethynyl Anthracene Dyad: Spin-Orbit Charge Transfer Intersystem Crossing and Triplet Excited-State Equilibrium. *J. Photochem. Photobiol. A* **2020**, *398*, 112573. [[CrossRef](#)]

Disclaimer/Publisher's Note: The statements, opinions and data contained in all publications are solely those of the individual author(s) and contributor(s) and not of MDPI and/or the editor(s). MDPI and/or the editor(s) disclaim responsibility for any injury to people or property resulting from any ideas, methods, instructions or products referred to in the content.